ARTICLES

Journal of Semiconductors
(2022) 43, 062803
doi: 10.1088/1674-4926/43/6/062803

Optimization of recess-free AlGaN/GaN Schottky barrier diode by TiN anode and current transport mechanism analysis

Hao Wu[1, 2], Xuanwu Kang[2, †], Yingkui Zheng[2], Ke Wei[2], Lin Zhang[3], Xinyu Liu[2], and Guoqi Zhang[1, †]

[1]The Institute of Future Lighting, Academy for Engineering and Technology, Fudan University (FAET), Shanghai 200433, China
[2]Institute of Microelectronics of the Chinese Academy of Sciences, Beijing 100029, China
[3]Beijing Const-Intellectual Core Technology Co. Ltd, Beijing 100029, China

Abstract: In this work, the optimization of reverse leakage current (I_R) and turn-on voltage (V_T) in recess-free AlGaN/GaN Schottky barrier diodes (SBDs) was achieved by substituting the Ni/Au anode with TiN anode. To explain this phenomenon, the current transport mechanism was investigated by temperature-dependent current–voltage (I–V) characteristics. For forward bias, the current is dominated by the thermionic emission (TE) mechanisms for both devices. Besides, the presence of inhomogeneity of the Schottky barrier height ($q\varphi_b$) is proved by the linear relationship between $q\varphi_b$ and ideality factor. For reverse bias, the current is dominated by two different mechanisms at high temperature and low temperature, respectively. At high temperatures, the Poole–Frenkel emission (PFE) induced by nitrogen-vacancy (V_N) is responsible for the high I_R in Ni/Au anode. For TiN anode, the I_R is dominated by the PFE from threading dislocation (TD), which can be attributed to the decrease of V_N due to the suppression of N diffusion at the interface of Schottky contact. At low temperatures, the I_R of both diodes is dominated by Fowler–Nordheim (FN) tunneling. However, the V_N donor enhances the electric field in the barrier layer, thus causing a higher I_R in Ni/Au anode than TiN anode, as confirmed by the modified FN model.

Key words: AlGaN/GaN; Schottky barrier diode; TiN; current transport mechanism

Citation: H Wu, X W Kang, Y K Zheng, K Wei, L Zhang, X Y Liu, and G Q Zhang, Optimization of recess-free AlGaN/GaN Schottky barrier diode by TiN anode and current transport mechanism analysis[J]. *J. Semicond.*, 2022, 43(6), 062803. https://doi.org/10.1088/1674-4926/43/6/062803

1. Introduction

AlGaN/GaN Schottky barrier diode (SBD) features excellent performance for high-power, high-frequency, and high-temperature applications, attributed to the outstanding properties of GaN material[1–5]. Recently, some researchers have demonstrated that AlGaN/GaN SBD has great potential for future wireless power transfer (WPT) applications[6–7]. The SBD converts the received RF signal into DC power, which determines the efficiency of the WPT system. To increase the conversion efficiency, AlGaN/GaN SBD requires a low turn-on voltage (V_T) while maintaining a low reverse leakage current (I_R).

The Schottky metal is well recognized to have a considerable impact on the V_T and I_R of Schottky junction (SJ). For AlGaN/GaN SBD, the most common electrode used as the anode is Ni/Au and TiN metal[2–5, 8–10]. Some researchers have compared the performance of AlGaN/GaN SJ based on Ni/Au and TiN Schottky metal. The related results show that the electrical characteristics of TiN-based SJ are better than Ni/Au-based SJ[11–13], but the mechanism is not well understood. A common explanation for this result is that the interaction between Ni and AlGaN(GaN) causes many defects or interface states, thus increasing the I_R[12–14]. To confirm this hypothesis, a clear understanding of the current transport mechanism is necessary to determine whether and how the related defects act on the electrical characteristics of SJ. However, the comparative analysis on the current transport mechanism of AlGaN/GaN SBDs with Ni/Au and TiN anodes is still lacking, and it would help obtain deeper physical insights into the impact of Schottky metal on the electrical properties of SBDs.

The recess-free technique can improve device uniformity and reliability by eliminating the plasma damage to the AlGaN barrier layer from the etching process[15–17]. In previous work, we have demonstrated high-performance recess-free AlGaN/GaN SBDs based on Ni/Au anode[16, 17]. However, recess-free AlGaN/GaN SBDs based on TiN anode have never been reported. The TiN anode can be compatible with CMOS processes[18], thus significantly reducing the fabrication cost of recess-free AlGaN/GaN SBDs.

In this paper, we have achieved the simultaneous improvement of V_T and I_R for recess-free AlGaN/GaN SBDs by substituting the Ni/Au anode with the TiN anode. The impact of Schottky metal on the electrical properties of SBDs is revealed by analyzing the current transport mechanism.

2. Device structure and fabrication

The epitaxial wafer is a commercial product from the Enkris Semiconductor, grown by MOCVD on a 3-inch sapphire <0001> substrate, consisting of a 1.5 μm C-doped GaN buffer layer, a 400 nm UID GaN channel layer, and a 7 nm $Al_{0.25}Ga_{0.75}N$ barrier layer. With a 24 nm LPCVD-SiN_x passivation (780 °C, with RCA pretreatment), the 2DEG channel in the access region was effectively preserved[19]. After passivation, the sheet resistance is reduced to 303 Ω/sq.

Correspondence to: X W Kang, kangxuanwu@ime.ac.com; G Q Zhang, G.Q.Zhang@tudelft.nl

Received 9 DECEMBER 2021; Revised 17 JANUARY 2022.

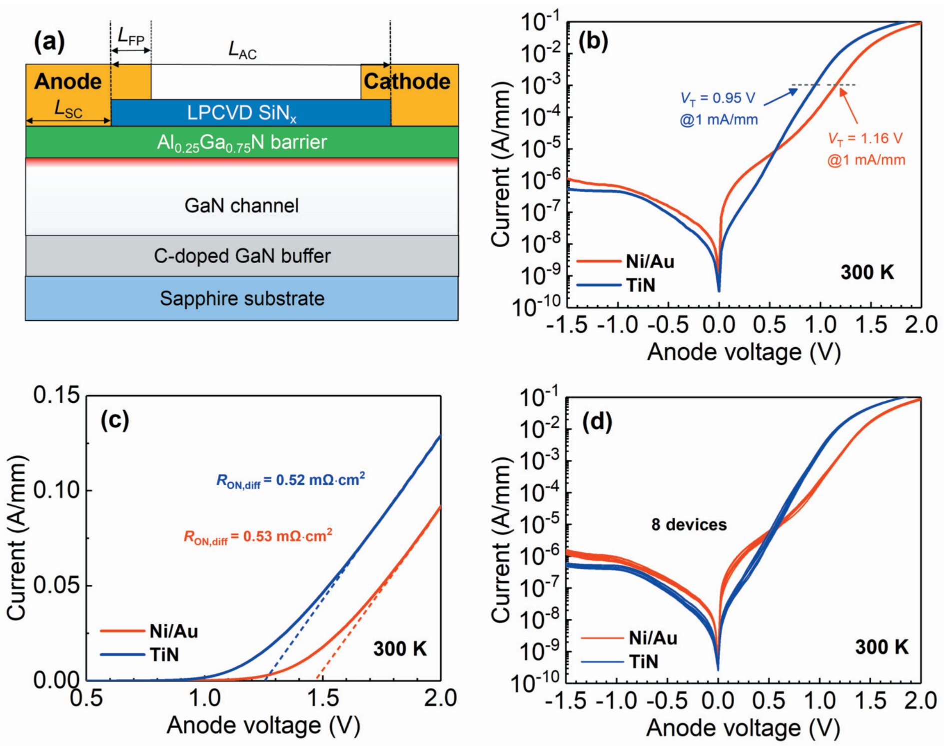

Fig. 1. (Color online) (a) Schematic cross-section of the fabricated recess-free AlGaN/GaN SBD. *I–V* characteristics of device A and B at RT on the (b) log scale and (c) linear scale. (d) *I–V* characteristics of 8 devices for A and B.

The schematic cross-section of SBD is shown in Fig. 1, and the device fabrication flow is the same except for the anode metal. First, the LPCVD SiN_x cap in anode and cathode region was opened with a fluorine-based ICP etch. Then, the metal layer of Ti/Al/Ni/Au (20/150/45/55 nm) was deposited, followed by rapid thermal annealing (RTA) at 870 °C for 50 s in N_2 ambient to form the ohmic cathode. Finally, Ni/Au (50 nm/150 nm) was deposited by evaporation to form the anode electrodes for device A, and TiN metal was deposited by reactive sputtering in Ar:N_2 (7 : 3 sccm) mixed gas atmosphere to form the anode electrodes for device B. The devices in this work have the same dimensions of $L_{SC}/L_{AC}/L_{FP}/W$ = 2/6/0.75/100 μm. The electrical characteristics of the device were measured with Keysight B1500A.

3. Overview of electrical characteristics

The *I–V* characteristics at room temperature (RT) on the log scale and linear scales are shown in Figs. 1(b) and 1(c), respectively. The SBD with TiN anode exhibits a low V_T of 0.94 V (defined as the voltage corresponding to current = 1 mA/mm), a low differential specific on-resistance ($R_{ON,diff}$) of 0.52 mΩ·cm² and a low I_R of ~ 0.5 μA/mm. Compared with SBD with TiN diode, the Ni/Au SBD exhibits similar $R_{ON,diff}$, while presenting a higher V_T of 1.16 V and a higher I_R of ~1 μA/mm. *I–V* curves of 8 devices are also plotted in Fig. 1(d), suggesting a good device uniformity attributed to the recess-free technique. The lower V_T in TiN SBD can be attributed to the difference between the work function of Ni (~5.15 eV) and of TiN (~4.7 eV)[13]. However, the lower I_R in TiN SBD is difficult to understand. To further explain the phenomenon, the temperature-related *I–V* measurement was carried out.

4. Current transport mechanisms at forward bias

The *I–V* characteristics of devices A and B measured from 223 to 473 K are shown in Figs. 2(a) and 2(b) and used to analyze the current transport mechanisms. The *I–V* characteristics of both devices can be divided into three regions, namely, region-I (low forward bias), region-II (high forward bias), and region-III (reverse bias). In region-I, the current show weak temperature and voltage dependence on the logarithmic axis, indicating that the tunneling-assisted transport mechanism dominates. Obviously, the tunneling effect in this region is more significant for Ni/Au SBD, although the metal work function of Ni is higher than that of TiN. The strong tunneling effect in Ni/Au SBD may be attributed to the interface states existing at the Ni/AlGaN interface caused by the interaction[12, 20]. In region-II, the current show strong temperature and voltage dependence, indicating that the thermionic emission (TE) is a possible transport mechanism. The equation of TE model can be simplified as[21]

$$I = SA^*T^2\exp\left(-\frac{q\varphi_b}{kT}\right)\exp\left(\frac{qV}{nkT}\right), \tag{1}$$

$$\ln I = \frac{qV}{nkT} + \ln\left(SA^*T^2\right) - \frac{q\varphi_b}{kT}, \tag{2}$$

where S is the SJ area, A^* is the effective Richardson constant of 30 A/(cm·K)² for $Al_{0.25}Ga_{0.75}N$[22], T is the absolute temperature, q is the fundamental electronic charge, V is the forward-bias voltage, k is the Boltzmann constant, $q\varphi_b$ is the apparent Schottky barrier height, and n is the ideality factor. Then, the experimental values of $q\varphi_b$ and the n can be extracted from intercepts and slopes of the forward ln*I* versus *V* plots in Figs. 2(a) and 2(b).

Fig. 2(c) shows the $q\varphi_b$ and n as a function of temperature. It can be observed that both $q\varphi_b$ and n show a strong temperature dependence for our devices. This observation is

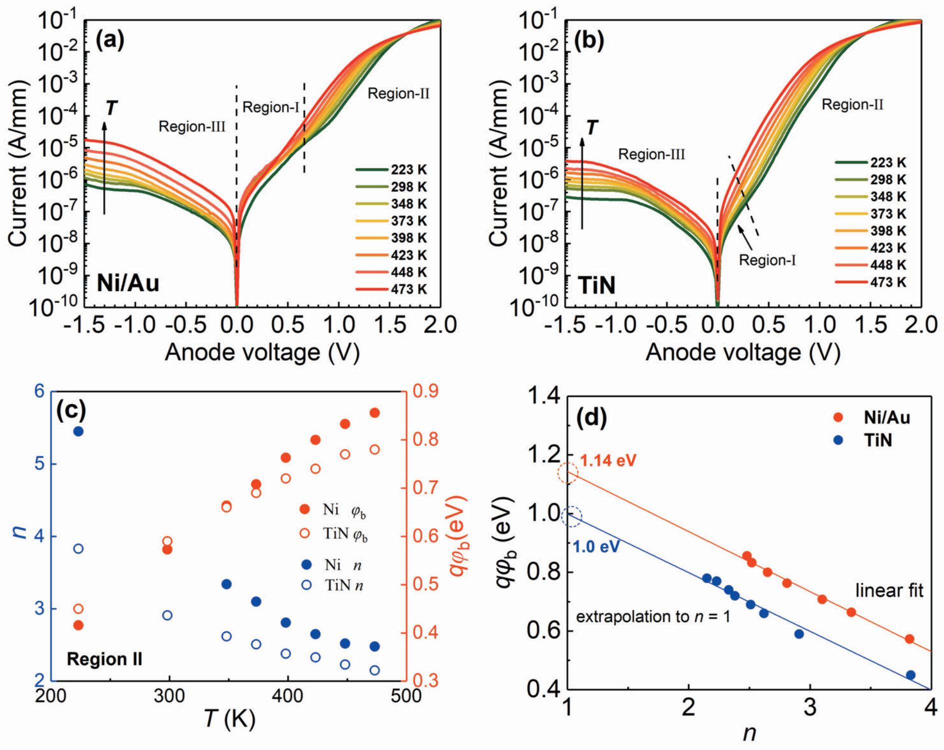

Fig. 2. (Color online) Temperature-dependent I–V characteristics of (a) device A and (b) device B. (c) Dependence of n and $q\varphi_b$ on the temperature for both devices. (d) The dependence of $q\varphi_b$ on n for two diodes; the extrapolation at $n = 1$ of the linear fit of the data gives a value of the mean barrier height.

inconsistent with the ideal TE mechanism, in which the $q\varphi_b$ and n should be almost constant with temperature. Besides, the calculated values of $q\varphi_b$ and n are also far from the ideal value ($n = 1$, $q\varphi_b = q\varphi_M - \chi_{AlGaN}$), especially at low temperatures. Several studies have suggested that such behavior is attributed to the spatial non-homogeneous distribution of the Schottky barrier height[23, 24]. At low temperature, the current is dominated by the low barrier regions because the electrons do not have enough energy to cross over the high barrier regions and thus lead to the low extracted $q\varphi_b$ at low temperatures. According to Schmitsdorf *et al.*[25] and Tung[26], the presence of inhomogeneity of the Schottky barrier height can be proved by the linear relationship between $q\varphi_b$ and n. Fig. 2(d) shows a linear reduction of $q\varphi_b$ with increasing n, which suggests the presence of inhomogeneity of the Schottky barrier height. By the extrapolation of $q\varphi_b$ to $n = 1$ in Fig. 2(d), the mean barrier height of 1.14 eV for Ni/Au anode and of 1.0 eV for TiN anode was determined. The extrapolated values agree with the experimental value of 1.10–1.30 eV for Ni/AlGaN SBD[27] and of 0.88–1.13 eV for TiN/AlGaN[13], thus validating our analysis. Moreover, TiN SBD exhibited lower n and higher $q\varphi_b$ compared with Ni/Au at low temperature (Fig. 2(c)), indicating the homogeneity of the Schottky barrier height of TiN/AlGaN contact is better than that of Ni/AlGaN contact. The poor homogeneity of Ni/AlGaN may be attributed to the defects induced by the interaction between Ni and AlGaN.

5. Current transport mechanisms at reverse bias

In region-III, it can be roughly seen that the temperature dependence of I_R varied with temperature for both devices, which indicated I_R could be dominated by different transport mechanisms at different ranges of temperature. To identify how many transport mechanisms work, the Arrhenius plots of I_R at $V_A = -0.5$ V are drawn in Fig. 3(a). Then, the activation energy (E_A) was extracted from the Arrhenius plots, as shown in Fig. 3(b).

The physical meaning of E_A is the energy barrier for electrons at the metal fermi-level to pass through the AlGaN barrier. Therefore, different E_A corresponds to different reverse leakage mechanisms. According to the extracted E_A in Fig. 3(b), the reverse leakage behavior can be roughly divided into two regions. At high temperatures, as temperature increases, the leakage current shows the apparent temperature dependence, indicating that the thermal emission process could dominate the leakage current in this region. The extracted E_A (< 0.6 eV) in this region (Fig. 3(b)) is much smaller than the Schottky barrier height reported in the literature (~ 1 eV)[11], suggesting that the emission of electrons is associated with the trap. At low temperatures, the temperature dependence of I_R is weaker, and E_A is almost zero (Fig. 3(b)), which indicates that the tunneling process could dominate the leakage current. A detailed analysis of reverse leakage mechanisms is presented in the next section.

Electric field (E) estimation is necessary to analyze I_R quantitatively. E across the AlGaN barrier layer can be calculated using the equation $E(V) = q[\sigma_p - n_s(V)]/\varepsilon_s\varepsilon_0$[28]. The fixed polarization charge density (σ_p) at the hetero-interface is estimated to be 1.35×10^{13} cm^{-2}[29]. $\varepsilon_s = 8.9$ [30] is the static dielectric constant of $Al_{0.25}Ga_{0.75}N$, and ε_0 is the vacuum dielectric constant. The 2DEG concentration (n_s) at the hetero-interface can be extracted from 1 MHz capacitance–voltage (C–V) curves in Fig. 4(a). The calculated E as a function of reverse bias is shown in Fig. 4(b), which will be used to analyze the leakage mechanism. Moreover, it can be seen in Fig. 4(a) that the pinch-off voltage ($V_{pin\text{-}off}$) in Ni SBD is higher than that in TiN

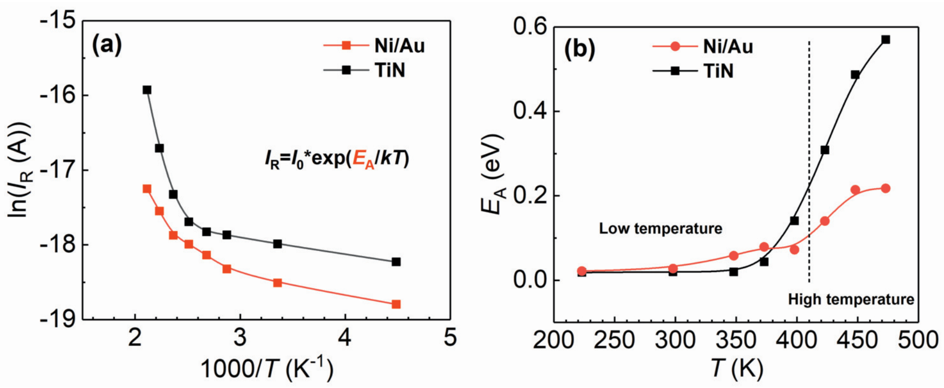

Fig. 3. (Color online) (a) Arrhenius plot of I_R for both devices. (b) E_A extracted from the Arrhenius plot.

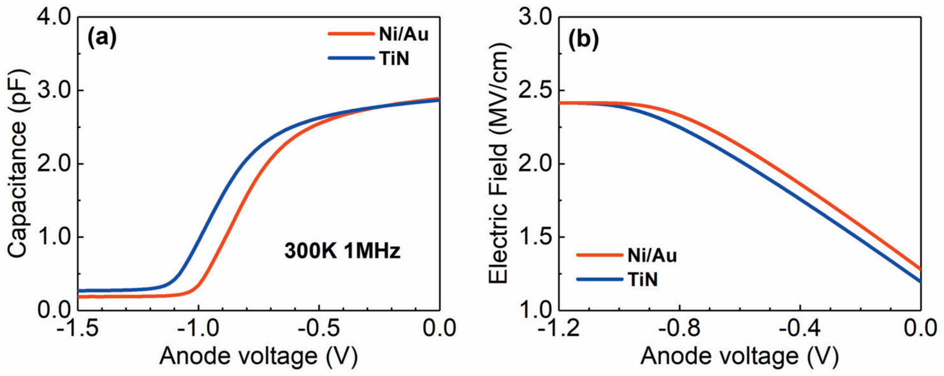

Fig. 4. (Color online) (a) 1 MHz $C–V$ characteristics under the reverse bias voltage. (b) Calculated $E–V$ characteristics under the reverse bias voltage.

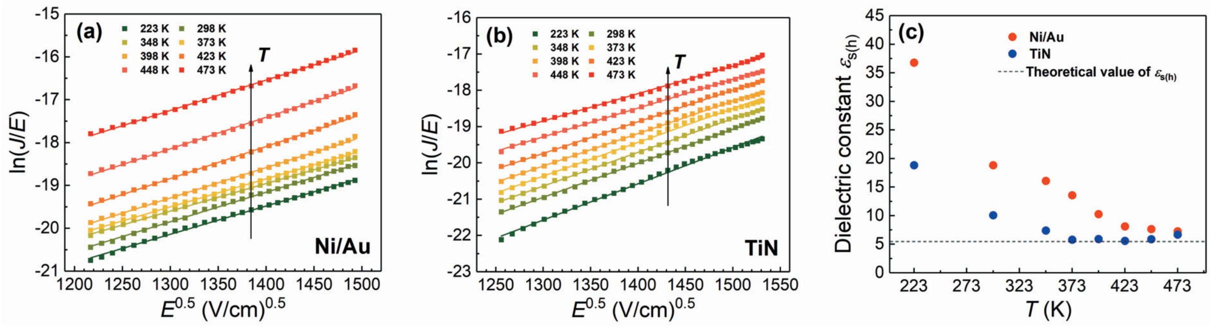

Fig. 5. (Color online) ln(J/E) versus $E^{0.5}$ at different temperatures for (a) device A and (b) device B. (c) Extracted $\varepsilon_{s(h)}$ at different temperatures for both devices.

SBD, which proves that the actual barrier height of Ni is higher than TiN.

5.1. Reverse leakage mechanisms at high temperature

Considering the strong temperature dependence at high temperatures, Poole–Frenkel emission (PFE) is the most probable carrier transport mechanism. The PFE refers to electric-field enhanced thermal emission from a trap state into a continuum of electronic, and the current density of PFE can be described as[31]:

$$J_{PF} = CE\exp\left[-\frac{q(\varphi_t - \sqrt{qE/\pi\varepsilon_{s(h)}\varepsilon_0})}{kT}\right], \tag{3}$$

where C is a constant associated with trap concentration, E is the electric field across the barrier, $q\varphi_t$ is the barrier height for the electron emission from the trap state, $\varepsilon_{s(h)}$ = 5.1[32] is the relative dielectric constant at high frequency for $Al_{0.25}Ga_{0.75}N$. Eq. (3) can be rearranged as given below

$$\begin{aligned}\ln(J_{PF}/E) &= \frac{q\sqrt{qE/\pi\varepsilon_{s(h)}\varepsilon_0}}{kT}\sqrt{E} - \frac{q\varphi_t}{kT} + \ln C \\ &= m(T)\sqrt{E} - \frac{q\varphi_t}{kT} + \ln C,\end{aligned} \tag{4}$$

or

$$\begin{aligned}\ln(J_{PF}/E) &= -\frac{q(\varphi_t - \sqrt{qE/\pi\varepsilon_{s(h)}\varepsilon_0})}{kT} + \ln C \\ &= -\frac{q\varphi_{eff}(E)}{kT} + \ln C.\end{aligned} \tag{5}$$

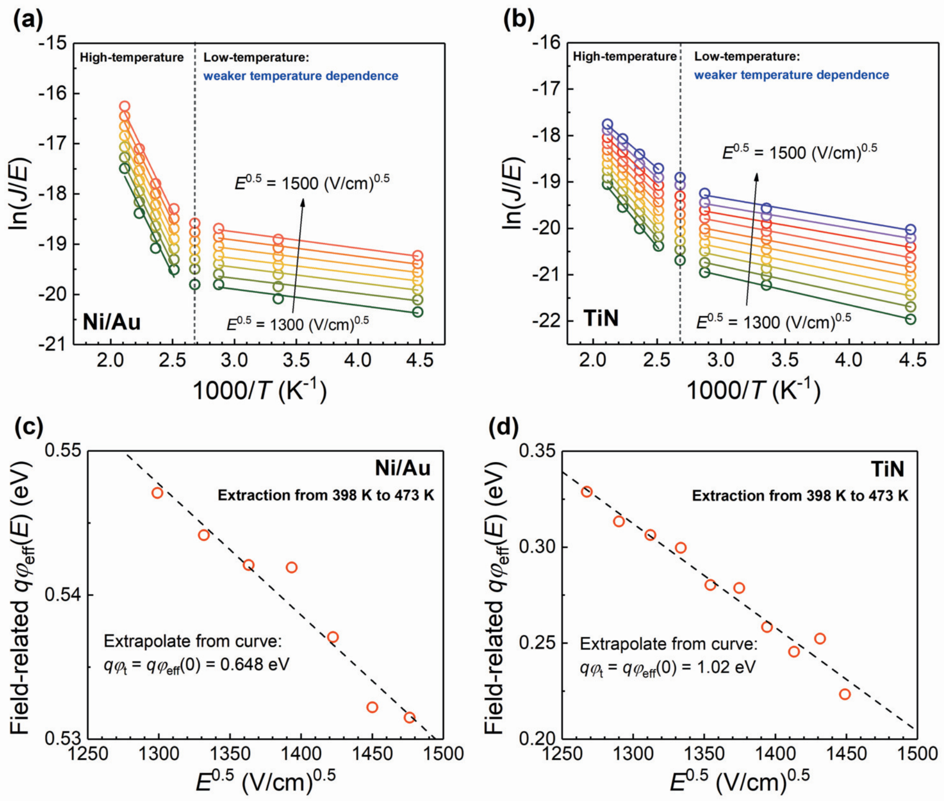

Fig. 6. (Color online) ln (J/E) versus 1000/T at various temperatures for (a) device A and (b) device B. Extracted $q\varphi_{\text{eff}}(E)$ at various temperatures for (c) device A and (d) device B.

From Eq. (4), ln(J_{PF}/E) should be a linear function of $E^{0.5}$. Figs. 5(a) and 5(b) show that the experimental plots of ln(J/E) versus $E^{0.5}$ fit well with the linear dependence at different temperatures for both devices, which proves the possibility of PFE. To further confirm the PFE, the $\varepsilon_{\text{s(h)}}$ in Eq. (4) were extracted from the $m(T)$ at different temperatures, as shown in Fig. 5(c). It is found that the $\varepsilon_{\text{s(h)}}$ extracted at high temperature (T > 400 K) is consistent with the theoretical value of $\text{Al}_{0.25}\text{Ga}_{0.75}\text{N}$, which strongly indicates that PFE is the dominant mechanism of I_{R} at high temperature. However, at medium and low temperatures (T < 400 K), the extracted $\varepsilon_{\text{s(h)}}$ is much higher than the theoretical value, indicating that different transport mechanisms dominate in this case.

To identify the defect origin of the trap-involved PFE, the extraction of $q\varphi_{\text{t}}$ is necessary. According to Eq. (5), ln(J_{PF}/E) should be a linear function of $1/T$, and $q\varphi_{\text{eff}}(E)$ can be extracted from the slope. The ln(J_{PF}/E) versus 1000/T plots were shown in Figs. 6(a) and 6(b), it can be seen that the data fit well with straight lines at high temperatures (T > 400 K) with various E. At medium and low temperatures (T < 400 K), the dependence of ln(J_{PF}/E) on temperature is weak, suggesting that the tunneling mechanism dominates in this case, although the data also follows a linear relationship. Then, the extracted E-related $q\varphi_{\text{eff}}(E)$ are shown in Figs. 6(c) and 6(d), and the $q\varphi_{\text{t}}$ obtained by extrapolating $q\varphi_{\text{eff}}(E)$ to zero electric field is 0.65 and 1.02 eV for Ni SBD and TiN SBD, respectively. The value of $q\varphi_{\text{t}}$ in Ni SBD and TiN SBD is respectively consistent with the energy level of threading dislocation (TD)[33, 34] and of N vacancy (V_{N})[35, 36] in AlGaN. Thus, the PFE from the V_{N} to conduction band and the TD to conduction band may dominate the I_{R} of Ni SBD and TiN SBD at high temperatures, respectively.

The difference in electrically active PFE defects between the two devices can be explained by the N diffusion mechanism based on Fick's law[12]. A significant difference in concentration or chemical potential between two materials facilitates the diffusion process from the region of high concentration to low concentration. The TiN anode with a high N concentration effectively suppresses the N diffusion process from the AlGaN layer to the Schottky metal, which reduces the V_{N} density in AlGaN, so PFE was dominated by natural defects such as threading dislocations. In contrast, the Ni anode with low N concentration facilitates the N diffusion process from the AlGaN layer to the Schottky metal, increasing the V_{N} density in AlGaN, so the V_{N} dominates the PFE. The N diffusion at Ni/AlGaN interface has been reported in as-fabricated HEMT[37], supporting our finding. Besides, the formation of Ni-nitrides has also been reported by annealing at the temperature of 200 °C[38]. In short, it can be considered that the PFE induced by the high-density V_{N} is responsible for the higher I_{R} in Ni SBD at high temperatures.

5.2. Reverse leakage mechanisms at low temperature

At low temperatures, the weak temperature dependence of I_{R} indicates that the tunneling process dominates. A possibility is Fowler–Nordheim (FN) tunneling, which is weakly related to temperature but strongly related to barrier height and electric field. The FN current density is given as[32]:

$$J_{\text{FN}} = AE^2\exp\left(-\frac{8\pi\sqrt{2m^*q}}{3hE}\varphi_{\text{b}}^{3/2}\right), \qquad (6)$$

where $A = ((q^2(m_0/m^*))/(8\pi h\varphi_{\text{b}}))$ is constant, h is Planck's constant, m_0 is the free-electron mass, $m^* \sim 0.27$ is the conduction band effective mass in the barrier layer, estimated by linear interpolation of the values in AlN and GaN[39]. Rearran-

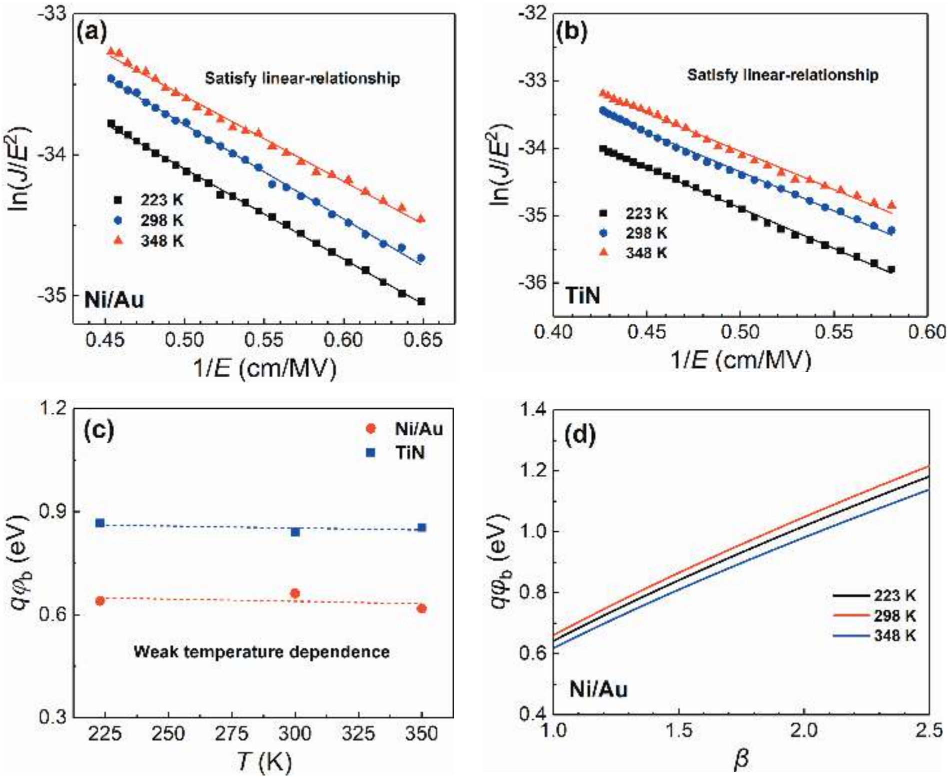

Fig. 7. (Color online) ln(J/E^2) versus $1/E$ at low temperature for (a) device A and (b) device B. (c) Extracted $q\varphi_b$ from the slope at various temperatures for both devices. (d) Impact of β on $q\varphi_b$ extracted by FN model for Ni SBD.

ging Eq. (7), we get

$$\ln(J_{FN}/E^2) \propto -\frac{8\pi\sqrt{2m^*q}\varphi_b^{3/2}/3h}{E}, \tag{7}$$

which indicates that the ln(J/E^2) versus $1/E$ plot should follow a linear dependency if FN tunneling process is the dominating mechanism, and the slope should be a weak function of T. Figs 7(a) and 7(b) show that the calculated ln(J/E^2) versus $1/E$ plot is very consistent with FN tunneling characteristics, indicating that FN tunneling dominates the leakage current at low temperatures for both devices. However, it is found that the $q\varphi_b$ of Ni SBD extracted from the slope is much lower than the $q\varphi_b$ of TiN SBD (Fig. 7(c)), which is inconsistent with the difference between the work function of Ni (5.15 eV) and TiN (4.7 eV). Moreover, the C–V characteristics (Fig. 4(a)) and the forward I–V characteristics (Figs. 2(c) and 2(d)) show that the $q\varphi_b$ of Ni SBD is higher than that of TiN SBD, which is also contradictory to Fig. 7(c).

It has been found that the ionization of V_N donor can cause the thin surface barrier (TSB) effect[40], thus leading to an increase of E in the barrier layer. Therefore, the low value of $q\varphi_b$ for Ni SBD extracted by the FN model may be attributed to the underestimation of the E. Considering the TSB effect, Eq. (7) should be corrected to:

$$\ln(J_{FN}/(\beta E)^2) \propto -\frac{8\pi\sqrt{2m^*q}\varphi_b^{3/2}/3h}{\beta E}, \tag{8}$$

where β is the electric field enhancement coefficient defined as the ratio of the actual electric field to the theoretical electric field. According to Eq. (8), the slope in Figs. 7(a) and 7(b) can be expressed as:

$$\text{slope} = -\frac{8\pi\sqrt{2m^*q}\varphi_b^{3/2}/3h}{\beta}. \tag{9}$$

Using Eq. (9), the relationship between β and $q\varphi_b$ for Ni SBD can be obtained, as shown in Fig. 7(d).

Fig. 7(d) shows that the extracted $q\varphi_b$ increases as β increases. When the β is between 1.5 and 2, the $q\varphi_{b0}$ for Ni SBD is close to the value reported in the literature [11, 27]. The large β indicates that the strong TSB effect exists in Ni SBD, which leads to the high I_R for Ni SBD compared to the TiN SBD at low temperatures. The TSB effect in Ni SBD is mostly caused by the donor-like V_N defect, which is introduced by the N diffusion process. For TiN SBD, the N diffusion process is effectively suppressed, and thus the extracted value of $q\varphi_b$ by the FN model is relatively normal (Fig. 7(c)).

Curiously, for reverse characteristics, the $q\varphi_b$ of TiN is higher than Ni (Fig. 7(c)), while for the forward characteristics, the $q\varphi_b$ of TiN is lower than Ni (Fig. 2(d)). This phenomenon can be explained as follows: at high forward bias, the quasi-Fermi level in semiconductor shifts above the level of V_N donor, and the ionized V_N will be neutralized, so the TSB effect in Ni/AlGaN will be weakened. Besides, the E in AlGaN barrier is decreased with forward bias, and the thermal emission related mechanism will gradually dominate the current transport, so the TSB effect has less influence on the forward characteristics.

In short, the carrier transport mechanisms of both devices are shown by the schematic energy band diagram in Fig. 8. According to the leakage mechanism analysis, it can be concluded that the main reason for the high I_R of Ni SBD is that the high-density V_N induced by the N diffusion enhances the PFE and FN tunneling. TiN SBD with high N concentrations is efficient to mitigate the N diffusion, thus obtaining a better trade-off between good V_T and I_R. Therefore, to re-

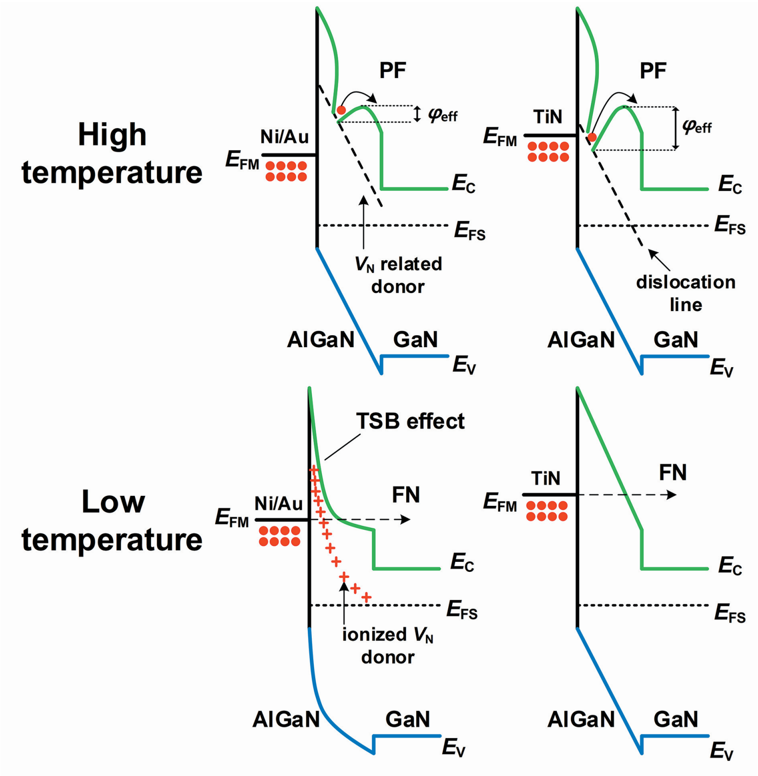

Fig. 8. (Color online) Schematic band diagram of carrier transport mechanisms at reverse bias for TiN SBD and Ni/Au SBD.

duce V_N density and improve SBD performance, conductive metal nitride, such as TiN, TaN, and WN_x, is more suitable as Schottky metal for AlGaN/GaN SBD.

6. Conclusion

In summary, we have comparatively investigated the reverse leakage mechanisms of recess-free AlGaN/GaN SBD with Ni/Au and TiN anodes. It is found that TiN SBD exhibits lower V_T and I_R than Ni SBD. For forward characteristics, the current of both devices is dominated by the TE mechanism. It is found that both $q\varphi_b$ and n show a strong temperature dependence. Such temperature dependence can be explained by the presence of inhomogeneity of the Schottky barrier height, which is proved by the linear relationship between $q\varphi_b$ and n. For reverse characteristics, two types of mechanisms work at different temperature ranges. At high temperatures, the I_R for Ni/Au anode is dominated by the PFE from V_N to the conduction band, while the I_R for TiN anode is dominated by the PFE from TD to the conduction band. The decrease of V_N can explain the observed low I_R in TiN SBD due to the suppression of N diffusion. At low temperatures, the I_R of both devices is dominated by FN tunneling. By modifying the FN model, we concluded that the electric field of the barrier layer in the Ni SBD is higher than in the TiN SBD, thus leading to the relatively higher FN leakage in Ni SBD. The TSB effect caused by V_N may be responsible for the increased electric field of the barrier layer in Ni SBD.

Acknowledgements

This work was supported in part by Natural Science Foundation of China (Grant No. 61804172), in part by GuangDong Province Key Technologies Research and Development Program (No. 2019B010128001) and in part by the Youth Innovation Promotion Association of CAS.

References

[1] Chen K J, Häberlen O, Lidow A, et al. GaN-on-Si power technology: Devices and applications. IEEE Trans Electron Devices, 2017, 64, 779

[2] Eblabla A, Li X, Alathbah M, et al. Multi-channel AlGaN/GaN lateral Schottky barrier diodes on low-resistivity silicon for sub-THz integrated circuits applications. IEEE Electron Device Lett, 2019, 40, 878

[3] Nela L, Kampitsis G, Ma J, et al. Fast-switching tri-anode Schottky barrier diodes for monolithically integrated GaN-on-Si power circuits. IEEE Electron Device Lett, 2020, 41, 99

[4] Xiao M, Ma Y W, Cheng K, et al. 3.3 kV multi-channel AlGaN/GaN Schottky barrier diodes with P-GaN termination. IEEE Electron Device Lett, 2020, 41, 1177

[5] Han S W, Song J N, Yoo S H, et al. Experimental demonstration of charge- balanced GaN super-heterojunction Schottky barrier diode capable of 2.8 kV switching. IEEE Electron Device Lett, 2020, 41, 1758

[6] Dang K, Zhang J C, Zhou H, et al. Lateral GaN Schottky barrier diode for wireless high-power transfer application with high RF/DC conversion efficiency: From circuit construction and device technologies to system demonstration. IEEE Trans Ind Electron, 2020, 67, 6597

[7] Dang K, Zhang J C, Zhou H, et al. A 5.8-GHz high-power and high-efficiency rectifier circuit with lateral GaN Schottky diode for wireless power transfer. IEEE Trans Power Electron, 2020, 35, 2247

[8] Lenci S, de Jaeger B, Carbonell L, et al. Au-free AlGaN/GaN power diode on 8-in Si substrate with gated edge termination. IEEE Electron Device Lett, 2013, 34, 1035

[9] Hu J, Stoffels S, Lenci S, et al. Performance optimization of Au-free lateral AlGaN/GaN Schottky barrier diode with gated edge termination on 200-mm silicon substrate. IEEE Trans Electron Devices, 2016, 63, 997

[10] Biscarrat J, Gwoziecki R, Baines Y, et al. Performance enhancement of CMOS compatible 600V rated AlGaN/GaN Schottky diodes on 200mm silicon wafers. 2018 IEEE 30th International Sym-

posium on Power Semiconductor Devices and ICs, 2018, 200
[11] Li Y, Ng G I, Arulkumaran S, et al. AlGaN/GaN high electron mobility transistors on Si with sputtered TiN gate. Phys Status Solidi A, 2017, 214, 1600555
[12] Kawanago T, Kakushima K, Kataoka Y, et al. Gate technology contributions to collapse of drain current in AlGaN/GaN Schottky HEMT. IEEE Trans Electron Devices, 2014, 61, 785
[13] Li L A, Nakamura R, Wang Q P, et al. Synthesis of titanium nitride for self-aligned gate AlGaN/GaN heterostructure field-effect transistors. Nanoscale Res Lett, 2014, 9, 590
[14] Kim H, Schuette M, Jung H, et al. Passivation effects in Ni/AlGaN/GaN Schottky diodes by annealing. Appl Phys Lett, 2006, 89, 053516
[15] Wu H, Kang X W, Zheng Y K, et al. Analysis of reverse leakage mechanism in recess-free thin-barrier AlGaN/GaN Schottky barrier diode. Jpn J Appl Phys, 2021, 60, 024002
[16] Kang X W, Wang X H, Huang S, et al. Recess-free AlGaN/GaN lateral Schottky barrier controlled Schottky rectifier with low turn-on voltage and high reverse blocking. 2018 IEEE 30th International Symposium on Power Semiconductor Devices and ICs, 2018, 280
[17] Kang X W, Zheng Y K, Wu H, et al. Thin-barrier gated-edge termination AlGaN/GaN Schottky barrier diode with low reverse leakage and high turn-on uniformity. Semicond Sci Technol, 2021, 36, 094001
[18] Sjoblom G, Westlinder J, Olsson J. Investigation of the thermal stability of reactively sputter-deposited TiN MOS gate electrodes. IEEE Trans Electron Devices, 2005, 52, 2349
[19] Sathaiya D M, Karmalkar S. Edge effects on gate tunneling current in HEMTs. IEEE Trans Electron Devices, 2007, 54, 2614
[20] Saadaoui S, Mongi Ben Salem M, Gassoumi M, et al. Electrical characterization of (Ni/Au)/$Al_{0.25}Ga_{0.75}N$/GaN/SiC Schottky barrier diode. J Appl Phys, 2011, 110, 013701
[21] Arehart A R, Moran B, Speck J S, et al. Effect of threading dislocation density on Ni/n-GaN Schottky diode I-V characteristics. J Appl Phys, 2006, 100, 023709
[22] Kim H, Song K M. Dislocation-related electron transport in Au Schottky junctions on AlGaN/GaN. Trans Electr Electron Mater, 2018, 19, 101
[23] Chatterjee A, Khamari S K, Dixit V K, et al. Dislocation-assisted tunnelling of charge carriers across the Schottky barrier on the hydride vapour phase epitaxy grown GaN. J Appl Phys, 2015, 118, 175703
[24] Peta K R, Park B G, Lee S T, et al. Analysis of electrical properties and deep level defects in undoped GaN Schottky barrier diode. Thin Solid Films, 2013, 534, 603
[25] Tung R T. Electron transport at metal-semiconductor interfaces: General theory. Phys Rev B, 1992, 45, 13509
[26] Schmitsdorf R F. Explanation of the linear correlation between barrier heights and ideality factors of real metal-semiconductor contacts by laterally nonuniform Schottky barriers. J Vac Sci Technol B, 1997, 15, 1221
[27] Qiao D, Yu L S, Lau S S, et al. Dependence of Ni/AlGaN Schottky barrier height on Al mole fraction. J Appl Phys, 1999, 87, 801
[28] Yan D W, Lu H, Cao D S, et al. On the reverse gate leakage current of AlGaN/GaN high electron mobility transistors. Appl Phys Lett, 2010, 97, 153503
[29] Ambacher O, Smart J, Shealy J R, et al. Two-dimensional electron gases induced by spontaneous and piezoelectric polarization charges in N- and Ga-face AlGaN/GaN heterostructures. J Appl Phys, 1999, 85, 3222
[30] Mahaveer Sathaiya D, Karmalkar S. Thermionic trap-assisted tunneling model and its application to leakage current in nitrided oxides and AlGaN/GaN high electron mobility transistors. J Appl Phys, 2006, 99, 093701
[31] Yeargan J R, Taylor H L. The Poole-Frenkel effect with compensation present. J Appl Phys, 1968, 39, 5600
[32] Zhang H, Miller E J, Yu E T. Analysis of leakage current mechanisms in Schottky contacts to GaN and $Al_{0.25}Ga_{0.75}N$/GaN grown by molecular-beam epitaxy. J Appl Phys, 2006, 99, 023703
[33] Fang Z Q, Farlow G C, Claflin B, et al. Effects of electron-irradiation on electrical properties of AlGaN/GaN Schottky barrier diodes. J Appl Phys, 2009, 105, 123704
[34] Fang Z Q, Look D C, Kim D H, et al. Traps in AlGaN/GaN/SiC heterostructures studied by deep level transient spectroscopy. Appl Phys Lett, 2005, 87, 182115
[35] Katsuno T, Kanechika M, Itoh K, et al. Improvement of current collapse by surface treatment and passivation layer in p-GaN gate GaN high-electron-mobility transistors. Jpn J Appl Phys, 2013, 52, 04CF08
[36] Johnstonea D K, Ahoujjab M, Yeoc Y K, et al. Deep centers and their capture barriers in MOCVD-grown GaN. MRS Proc, 2001, 692, H2.7.1
[37] Whiting P G, Holzworth M R, Lind A G, et al. Erosion defect formation in Ni-gate AlGaN/GaN high electron mobility transistors. Microelectron Reliab, 2017, 70, 32
[38] Koehler A D, Nepal N, Anderson T J, et al. Atomic layer epitaxy AlN for enhanced AlGaN/GaN HEMT passivation. IEEE Electron Device Lett, 2013, 34, 1115
[39] Xu Y N, Ching W Y. Electronic, optical, and structural properties of some wurtzite crystals. Phys Rev B, 1993, 48, 4335
[40] Hasegawa H, Inagaki T, Ootomo S, et al. Mechanisms of current collapse and gate leakage currents in AlGaN/GaN heterostructure field effect transistors. J Vac Sci Technol B, 2003, 21, 1844

Hao Wu received the MS degree in Integrated Circuit Engineering from North China University of Technology, Beijing, China, in 2019. And he is now pursuing the PhD degree in Fudan University, Shanghai, China. Meanwhile, studying at Institute of Microelectronics of Chinese Academy of Sciences, Beijing, China. His research interests include current conduction mechanism for AlGaN/GaN diode and reliability for AlGaN/GaN diode.

Xuanwu Kang received a PhD degree from the Fudan University, Shanghai, China, in 2021. He is currently with Institute of Microelectronics, Chinese Academy of Sciences, Beijing, China. His research interests include the GaN device for wireless power transfer and power electronics.

Guoqi Zhang (M'03–F'14) received a PhD degree from the Delft University of Technology, Delft, the Netherlands, in 1993. He was with NXP Semiconductors, Eindhoven, the Netherlands, as the Senior Director of Technology Strategy, until 2009, and was a Philips Research Fellow until May 2013. He is currently a Chair Professor of micro/nanoelectronics system integration and reliability with the Delft University of Technology. He has authored/coauthored more than 400 scientific publications. His research interest covers multilevel heterogeneous system integration and packaging, wide-bandgap semiconductors sensors and components, multiphysics and multiscale modeling of micro/nanoelectronics, and digital twin for mission critical multifunctional electronics components and systems.